ACS APPLIED BIO MATERIALS
Cite This: ACS Appl. Bio Mater. 2019, 2, 769−776
Article
www.acsabm.org

Antimicrobial Peptide-Conjugated MoS_2-Based Nanoplatform for Multimodal Synergistic Inactivation of Superbugs

Salma Begum, Avijit Pramanik, Kaelin Gates, Ye Gao, and Paresh Chandra Ray*

Department of Chemistry and Biochemistry, Jackson State University, Jackson, Mississippi 39217, United States

Supporting Information

ABSTRACT: Development of new antibacterial therapeutic materials is becoming increasingly urgent due to the huge threat of superbugs, which are responsible for more than half of a million deaths each year in this world. Here, we report the development of a novel nanobiomaterial based on a melittin antimicrobial peptide (AMP)-attached transition metal dichalcogenide MoS_2-based theranostic nanoplatform. The reported nanoplatform has a capability for targeted identification and synergistic inactivation of 100% multidrug-resistant superbugs by a combined photo thermal therapy (PTT), photodynamic therapy (PDT), and AMP process. A novel approach for the design of a melittin antimicrobial peptide-attached MoS_2-based nanoplatform is reported, which emits a very bright and photo stable fluorescence. It also generates heat as well as reactive oxygen species (ROS) in the presence of 670 nm near-infrared light, which allows it to be used as a PTT and PDT agent. Due to the presence of AMP, multifunctional AMP exhibits a significantly improved antibacterial activity for superbugs via a multimodal synergistic killing mechanism. Reported data demonstrate that nanoplatforms are capable of identification of multidrug-resistant superbugs via luminescence imaging. Experimental results show that it is possible to kill only ∼45% of superbugs via a MoS_2 nanoplatform based on PTT and PDT processes together. On the other hand, killing less than 10% of superbugs is possible using melittin antimicrobial peptide alone, whereas 100% of methicillin-resistant *Staphylococcus aureus* (MRSA), drug-resistant *Escherichia coli* (*E. coli*), and drug-resistant *Klebsiella pneumoniae* (KPN) superbugs can be killed using antimicrobial peptide-attached MoS_2 QDs, via a synergistic killing mechanism. Mechanisms for possible synergistic killing of multidrug-resistant superbugs have been discussed.

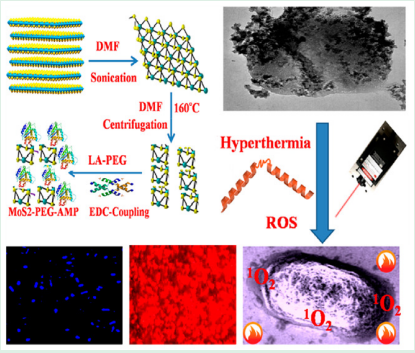

KEYWORDS: *melittin antimicrobial peptide-attached MoS_2-based nanoplatform, theranostic transition metal dichalcogenide, photo thermal therapy, photodynamic therapy, multimodal therapy for multidrug-resistant superbugs*

1. INTRODUCTION

Multidrug-resistant superbugs, which are nightmares for medical treatment, are responsible for more than half of a million deaths in this world every year.[1−3] Due to a high frequency of multidrug-resistant superbug infections, there is an urgent need for alternate approaches for killing superbugs.[1−8] Recently, we and other groups have reported nanomaterial-based photoinduced killing of bacteria via photodynamic therapy (PDT) and photo thermal therapy (PTT) processes.[9−21] External light-triggered PTT has been extensively explored for cancer and pathogens because of its lesser side effects and high specificity.[8−10,13,19] Similarly, PDT causes also external light-triggered destruction of cancer cells and pathogens, by producing highly reactive oxygen species (ROS).[6−14] Recently, therapeutic applications have shifted away from monotherapy to an external NIR-light-triggered combined PTT/PDT therapy approach. It is now well-reported that the combined therapy process greatly enhances the therapeutic efficacy with a much lower toxic side effect.[8−16] Two-dimensional (2D) MoS_2 is now reported as promising building blocks for photothermal agents.[22−43] For developing a PTT/PDT/antimicrobial peptide (AMP)-based multimodal MDRB killing theranostic material, here we report the development of a nanoplatform based on a melittin antimicrobial peptide-attached transition metal dichalcogenide MoS_2 nanoplatform. Reported theranostic material has the capability for selective identification and destruction of superbugs.

It also exhibits a significantly improved antibacterial activity for superbugs via a multimodal synergistic killing mechanism. In our design, a water-soluble MoS_2-based nanoplatform has been used as a photoluminescence probe for luminescence bioimaging of superbugs. Due to photothermal properties and ROS generation capability, a MoS_2 nanoplatform has been used as an external NIR-light-triggered combined photothermal and photodynamic killing agent for superbugs. On the other hand, melittin antimicrobial peptide has been used to kill superbugs by pore formation.[44−48] Reported data demonstrate that 100% of *E. coli*, KPN, and MRSA superbugs can be killed using melittin antimicrobial peptide-attached MoS_2 nanoflakes,

Received: October 21, 2018
Accepted: December 24, 2018
Published: December 24, 2018

DOI: 10.1021/acsabm.8b00632
ACS Appl. Bio Mater. 2019, 2, 769−776

via a possible synergistic killing mechanism. However, our reported results show that the PDT/PTT combined killing using MoS_2 nanoflakes is not enough to completely destroy superbugs in a 10^5/mL dose level. We observed less than 50% PDT/PTT combined killing of different superbugs using MoS_2 nanoflakes. To overcome the above limitation, we developed a melittin antimicrobial peptide-attached MoS_2-based theranostic nanoplatform.

In our design, we developed a melittin antimicrobial peptide-attached MoS_2-based theranostic nanoplatform, where the melittin antimicrobial peptide can kill superbugs via pore formation.[44−48] However, experimental data indicate that only the melittin antimicrobial peptide can kill 10−15% of superbugs. On the other hand, the melittin antimicrobial peptide-attached MoS_2-based theranostic nanoplatform can be used to kill 100% of superbugs by using a synergistic killing mechanism.

2. RESULTS AND DISCUSSION

2.1. Design of Melittin Antimicrobial Peptide-Attached PEG-MoS_2-AMP Nanoplatforms. We developed a PEG-MoS_2-AMP nanoplatform using a three-step method, as shown in Scheme 1. Detailed synthetic procedures have been described in the Supporting Information. At the end, a PEG-MoS_2-AMP nanoplatform was characterized by different microscopic and spectroscopic techniques as reported in Figure 1A−I. Figure 1A shows the tunneling electron microscopy data for MoS_2 nanosheets. Figure 1B shows TEM data for the PEG-MoS_2-AMP nanoplatform, whose size is ∼15 ± 5 nm. To understand better the size distribution in solution phase, we also performed a dynamic light scattering (DLS) experiment, which shows that the nanoplatform size is ∼13 ± 5 nm. HRTEM data reported in Figure 1B shows that the fringe lattice spacing is around 0.27 nm. The HRTEM data is also in agreement with the X-ray diffraction (XRD) results, reported in Figure 1D. Energy-dispersive X-ray (EDX) data reported in Figure 1B shows the elemental analysis for the PEG-MoS_2-AMP nanoplatform. To find out the colloidal stability of MoS_2-PEG, we measured the size of MoS_2-PEG with time up to 60 days, using DLS measurements. We also performed the same colloidal stability experiment for MoS_2, only without PEG. As shown in Figure S1, the colloidal stability for MoS_2-PEG is much better than that for only MoS_2.

Scheme 1. Synthetic Procedure Used for the Development of an Antimicrobial Peptide-Attached MoS_2-Based Nanoplatform

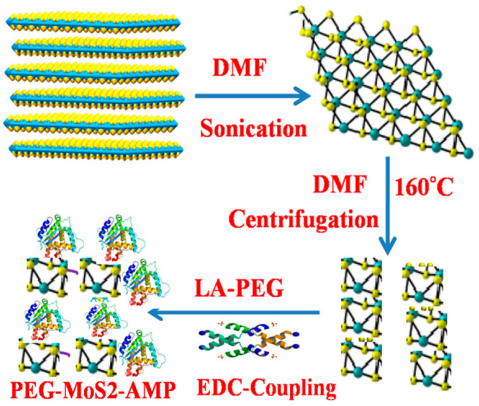

Figure 1D shows the XRD pattern of the PEG-MoS_2-AMP nanoplatform, which shows four characteristic peaks of PEG-MoS_2-AMP nanoplatforms corresponding to (002), (100), (104), and (110) planes.[22−30] Figure 1E shows the absorption spectra for the PEG-MoS_2-AMP nanoplatform, which shows the broad absorption band between 500 and 700 nm, which can be attributed to C and D excitonic bands.[22−30] Figure 1F shows the FTIR spectra from PEG-MoS_2-AMP, which indicate the presence of an amide-N−H stretch at ∼3500 cm^{-1}, amide-I band at ∼1650 cm^{-1}, amide-II band at ∼1540 cm^{-1}, and amide-III bands at ∼1300 cm^{-1}. All of the observed amide bands clearly indicate the presence of AMP in the nanoplatform. As shown in Figure 1G, we also performed Raman characterization for the PEG-MoS_2-AMP nanoplatform, where both Raman bands for MoS_2 are observed.[22−30] Figure 1H shows the photoluminescence behavior for PEG-MoS_2 and the PEG-MoS_2-AMP nanoplatform upon irradiation of 285 nm UV light. As shown in Figure 1H, PEG-MoS_2 exhibits one photoluminescence peak at 405 nm, whereas the PEG-MoS_2-AMP nanoplatform exhibits two photoluminescence peaks. The observed first photoluminescence peak at 340 nm is due to the tryptophan residue in melittin AMP, and the observed second photoluminescence peak at 405 nm is due to MoS_2. The amount of melittin conjugated on the nanoplatform was estimated by measuring the change in the photoluminescence intensity at 340 nm, which is due to the tryptophan residue of melittin, in the supernatant before and after conjugation. For this purpose, after conjugation with the nanoplatform, the excess melittin AMP was separated from the nanoplatform by centrifugation at 100 000 rpm for several hours. From the fluorescence measurement, before and after conjugation, we estimated that the amount of melittin conjugated on the platform was ∼2.8 ± 0.4 μg/mL. The inserted figure in Figure 1H clearly shows the blue light emission from the PEG-MoS_2-AMP nanoplatform. The photoluminescence quantum yield for the PEG-MoS_2-AMP nanoplatform was determined to be 12.8%, with respect to quinine sulfate as a standard.

2.2. Use of Melittin Antimicrobial Peptide-Attached PEG-LA-MoS_2 QDs for MDRB Imaging and Synergistic Killing. For the detection and killing of different MDRBs, we mixed the PEG-MoS_2-AMP nanoplatform with different superbugs (10^5 CFU/mL) separately. After the nanoplatform was gently mixed for several minutes, we performed centrifugation for the separation of PEG-MoS_2-AMP nanoplatform-bound MDRBs. We characterized PEG-MoS_2-AMP nanoplatform-bound MDRBs using fluorescence and microscope data, reported in Figure 2A−D. Figure 2A,B shows PEG-MoS_2-AMP-bound *E. coli* and MRSA, respectively. It is well-documented that melittin AMP targets bacterial cell membranes via binding with the cell surface, lipid components, and phospholipid groups. We believe that the PEG-MoS_2-AMP nanoplatform binds with bacteria via anionic groups on membranes. Since the size of bacteria is about 1 μm, and the size of the nanoplatform is only around 15 nm, we observed that a huge amount of the PEG-MoS_2-AMP nanoplatform is bound on the bacteria surface as shown in Figure 2A,B. The reported blue fluorescence image, as shown in Figure 2C,D, indicates that the PEG-MoS_2-AMP nanoplatform is bound with different MDRBs.

Before the imaging experiment, we performed biocompatibility experiments for MoS_2-PEG. Experimental details have

DOI: 10.1021/acsabm.8b00632
ACS Appl. Bio Mater. 2019, 2, 769−776

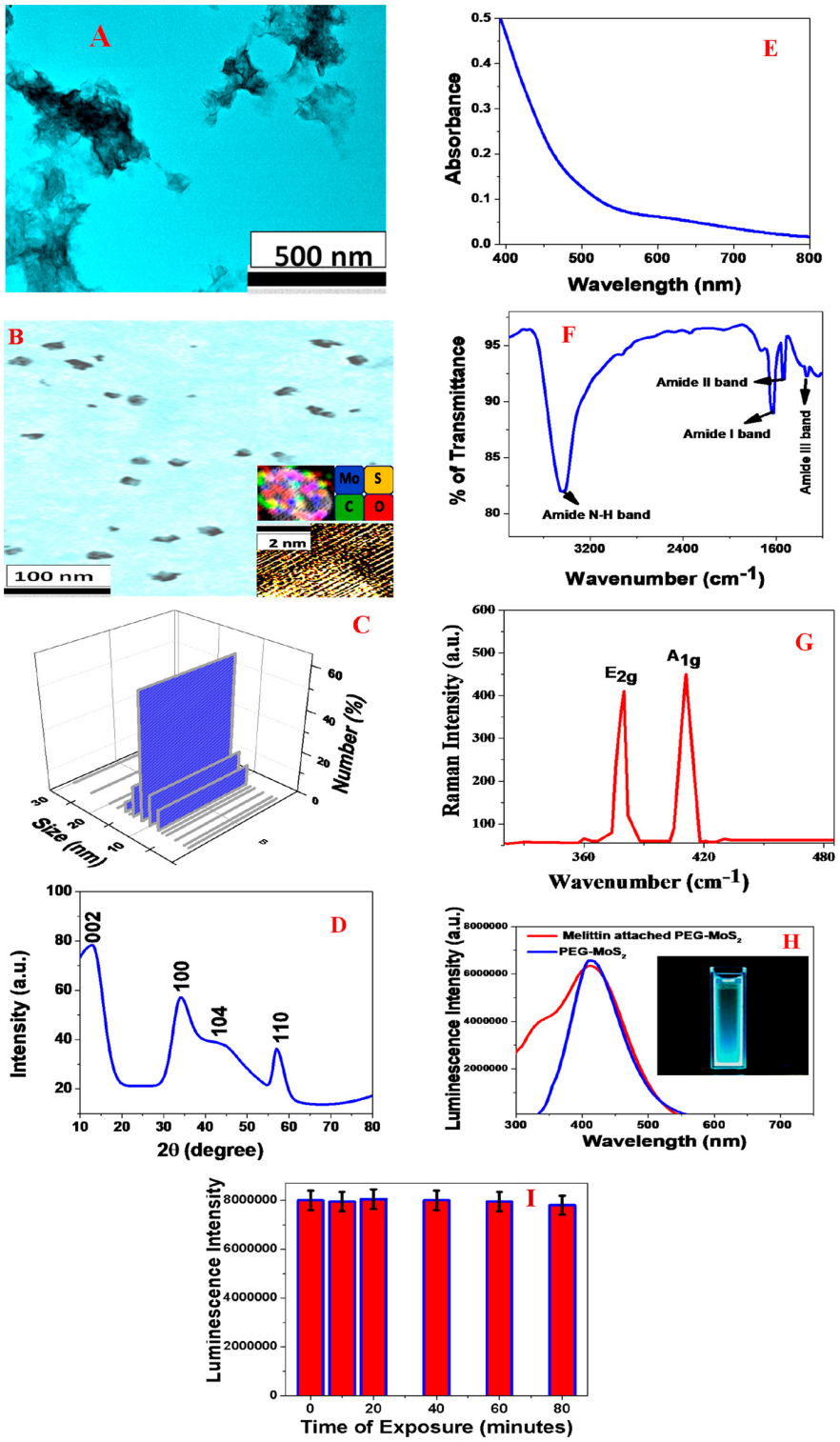

Figure 1. (A) TEM image of a 2D MoS_2 sheet. (B) TEM image shows the morphology of the freshly prepared PEG-MoS_2-AMP nanoplatform. Inserted HRTEM and EDX data show the lattice fringe and elemental analysis for nanoplatforms. (C) Size distribution data for the nanoplatform, measured by DLS. (D) XRD spectra from the PEG-MoS_2-AMP nanoplatform. (E) Absorption spectra from the PEG-MoS_2-AMP nanoplatform. (F) FTIR spectra of the nanoplatform. (G) Raman spectra of the PEG-MoS_2-AMP nanoplatform. (H) Photoluminescence spectra for PEG-MoS_2 and the PEG-MoS_2-AMP nanoplatform upon irradiation at 285 nm UV light. (I) Variation of the photo luminescence intensity from the PEG-MoS_2-AMP nanoplatform with time, during the photothermal experiment.

been reported before.[6,16,21,36] Reported data in Figure 3A–C indicates a good biocompatibility for MoS_2-PEG QDs.

To understand the biocompatibility of MoS_2 without PEG, we also performed the same biocompatibility experiments for

DOI: 10.1021/acsabm.8b00632
ACS Appl. Bio Mater. 2019, 2, 769–776

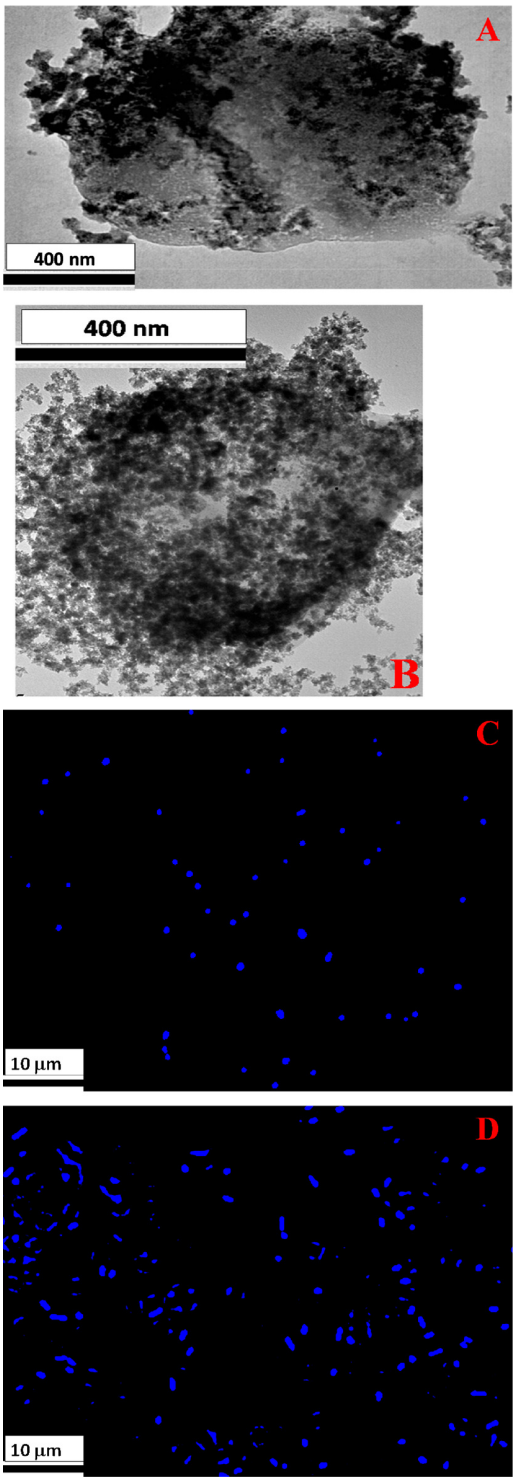

Figure 2. (A) TEM data indicating that the PEG-MoS_2-AMP nanoplatform is attached to *E. coli*. (B) TEM data showing that the PEG-MoS_2-AMP nanoplatform is attached to MRSA. (C) Fluorescence image of PEG-MoS_2-AMP nanoplatform-bound MRSA. The blue fluorescence in the image originates from the nanoplatform, which is attached to MRSA. (D) Fluorescence image of PEG-MoS_2-AMP nanoplatform-bound CRE *Escherichia coli*. The blue fluorescence in the image originates from the nanoplatform, which is attached to CRE *Escherichia coli*.

MoS_2 only. As reported in Figure S2, around 93−95% cell viability was observed, which indicates that the biocompatibility of MoS_2-PEG QDs is better than that of MoS_2 only.

We determined the minimum inhibitory concentrations (MICs) for melittin antimicrobial peptide against *Escherichia coli*, ESBL-producing *Klebsiella pneumoniae* (KPN), and MRSA via determining the bacterial growth using the ELISA technique. Experimental details are reported in the Supporting Information. From the experimental results, we determined that the MIC value for the melittin antimicrobial peptide is 12 μg/mL for MRSA. On the other hand, the MIC value for the melittin antimicrobial peptide is 58 μg/mL for CRE *Escherichia coli* and the MIC value for the melittin antimicrobial peptide is 64 μg/mL for ESBL-producing *Klebsiella pneumoniae* (KPN). The reported MIC value is the lowest concentration of the melittin antimicrobial peptide necessary for exhibiting no visible growth for up to 24 h of incubation.

Next, we performed an NIR light exposure experiment to find out whether our melittin antimicrobial peptide-attached PEG-MoS_2-AMP nanoplatform can be used for multimodal killing, as shown in Scheme 2. Experimental details have been reported before.[6,16,21,36] Figure 3A,B shows the ESBL-producing *Klebsiella pneumoniae* (KPN) killing efficiency, which indicates that 100% of ESBL-producing *Klebsiella pneumoniae* (KPN) bacteria are dead, when KPN was exposed to 670 nm light for 10 min. As reported in Figure 3D,E, we also used Live/Dead BacLight molecular probes to determine the amount of dead or live ESBL-producing *Klebsiella pneumoniae* (KPN) bacteria and other MDRBs. Figure 3D indicates ESBL-producing *Klebsiella pneumoniae* (KPN) bacteria are alive without the PEG-MoS_2-AMP nanoplatform, whereas Figure 3E shows that 100% of ESBL-producing *Klebsiella pneumoniae* (KPN) bacteria are dead when the PEG-MoS_2-AMP nanoplatform is present. Figure 3F,G shows the light-induced antibacterial activity of the melittin antimicrobial peptide-attached PEG-MoS_2-AMP nanoplatform against different superbugs. Reported experimental data clearly indicate that almost 100% of superbugs can be killed, which is due to the NIR-light-induced multimodal killing processes. Next, to find out whether the multimodal killing mechanism for different MDRBs is greatly superior to the single-mode killing mechanism, we designed several different experiments.

At first, the antibacterial activity experiment was performed for MDRB using only the melittin antimicrobial peptide (3 μg/mL), with and without light. As reported in Figure 3F−H, less than 10% of superbugs are killed and the antibacterial activity amount is independent of NIR light. These reported results indicate that the antibacterial activity by the antimicrobial peptide-attached PEG-MoS_2-AMP nanoplatform without light is due to antimicrobial peptide. Similarly, we also performed antibacterial activity measurements using a PEG-MoS_2-AMP nanoplatform and 670 nm light. As shown in Figure 3C, less than 1% of MDRB was killed, which indicates that PEG-MoS_2 nanoflakes are not cytotoxic without light. As is shown in Figure 3E, around 15% of MRSA was killed when the melittin antimicrobial peptide is present and it is due to the lower MIC value for MRSA, as we discussed before. The observed MDRB antibacterial activity for MRSA is due to the formation of pores on the MDRB membrane,[45−48] as reported in Figure 3K,L.

To understand the membrane pore formation better, we performed a bacterial ATP leakage experiment using the ATP

DOI: 10.1021/acsabm.8b00632
ACS Appl. Bio Mater. 2019, 2, 769−776

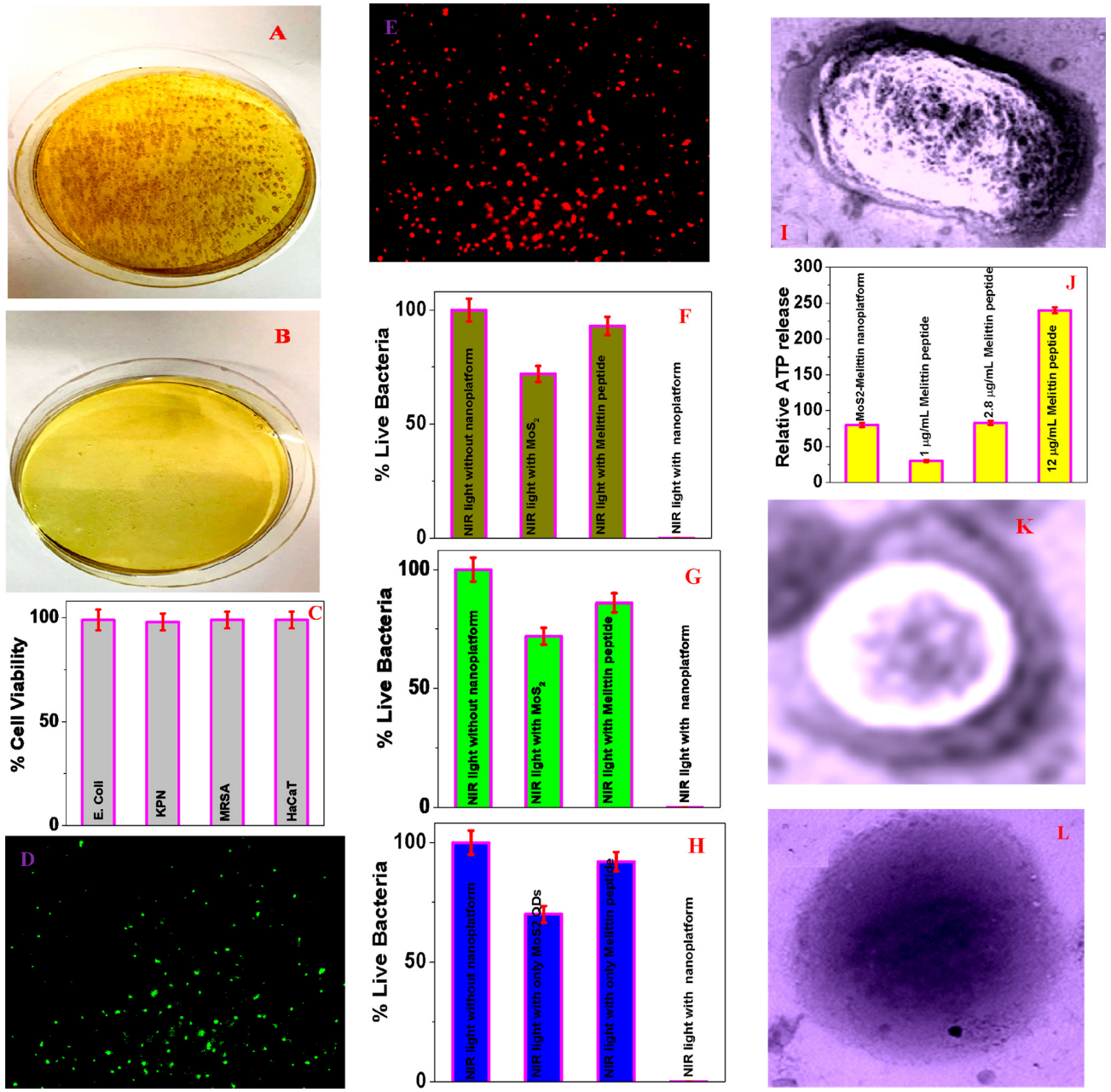

Figure 3. (A, B) Measured 670 nm light-induced KPN inactivation efficiency, (A) without the PEG-MoS_2-AMP nanoplatform and (B) with the PEG-MoS_2-AMP nanoplatform and 670 nm light. (C) Biocompatibility of PEG-MoS_2 (10 μg/mL) against CRE *Escherichia coli*, KPN, MRSA, and normal skin HaCaT cells. (D, E) Killing efficiency of KPN measured by Live/Dead BacLight molecular probes. Fluorescence images are overlaid images of the FITC and PI channels. (D) Without the PEG-MoS_2-AMP nanoplatform. (E) With the PEG-MoS_2-AMP nanoplatform. (F) KPN killing efficiency using only NIR light, PEG-MoS_2 nanoflakes and light, melittin AMP (3 μg/mL) and light, and PEG-MoS_2-AMP nanoplatform and light. (G) MRSA inactivation efficiency using only 670 nm light, PEG-MoS_2 nanoflakes and light, melittin antimicrobial peptide (3 μg/mL) and light, and PEG-MoS_2-AMP nanoplatform and light. (H) CRE *Escherichia coli* inactivation efficiency using only 670 nm light, PEG-MoS_2 nanoflakes and light, melittin antimicrobial peptide (3 μg/mL) and light, and PEG-MoS_2-AMP nanoplatform and light. (I) The TEM image clearly shows membrane damage on the KPN bacteria surface by the PEG-MoS_2-AMP nanoplatform in the presence of NIR light. (J) Relative cellular ATP leakage percentage for MRSA bacteria. (K) TEM image of MRSA after exposure to light and the PEG-MoS_2-AMP nanoplatform. (L) TEM image of MRSA after exposure to light, when the PEG-MoS_2-AMP nanoplatform is absence.

determination kit. This ATP determination kit is based on the luminescence results from the firefly luciferase enzyme. For this experiment, PEG-MoS_2 without NIR light was used as a control because our experimental data shows no toxicity from MoS_2. As reported in Figure 3J, the ATP leakage experiment clearly shows a melittin peptide concentration-dependent leakage of cellular ATP in the case of MRSA, which indicates the cellular membrane damage in the presence of AMP. Reported data also shows that, although the MIC value for the melittin antimicrobial peptide is 12 μg/mL for MRSA, we noted a high amount of leakage of cellular ATP even at a concentration of 2.8 μg/mL. Our experimental data, as

DOI: 10.1021/acsabm.8b00632
ACS Appl. Bio Mater. 2019, 2, 769−776

Scheme 2. Superior Antibacterial Activity of Our Developed Nanoplatform for Superbugs via Combined Photo Thermal Therapy (PTT), Photodynamic Therapy (PDT) and AMP Process

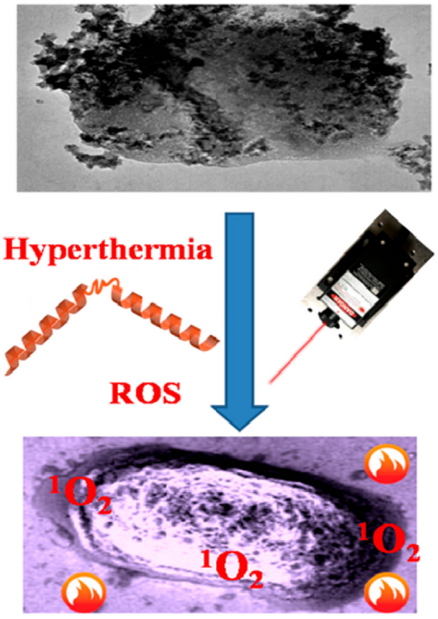

reported in Figure 3J, indicates that the leakage of cellular ATP in the presence of a nanoplatform is very similar to the value for the melittin antimicrobial peptide at a concentration of 2.8 μg/mL .

Next, we also performed the experiment to understand PTT and PDT combined therapy activity by the PEG-MoS_2-AMP nanoplatform without an antimicrobial peptide. As reported in Figure 3D,F, around 45% of antibacterial activity was observed for different superbugs, respectively, using PEG-MoS_2-AMP nanoplatform-based PDT and PTT. To understand the photothermal killing process using the PEG-MoS_2-AMP nanoplatform, we measured the temperature variation during the light-induced killing process. Experimental details have been reported before.[22,23,26−29] As shown in Figure 4A, experimental data shows that the temperature increased to about 43 °C when the PEG-MoS_2-AMP nanoplatform with β-lactamase (ESBL)-producing *Klebsiella pneumoniae* (KPN) was exposed to 1.3 W cm^{-2} power NIR light. As reported in Figure 4A, the temperature increase amount is about the same in the presence or absence of the melittin antimicrobial peptide. The temperature increased to only 29 °C in the absence of the PEG-MoS_2-AMP nanoplatform, when only buffer was used. Our reported data clearly show that the PEG-MoS_2-AMP nanoplatform has the capability to kill MDRB by photothermal killing. Since the absorption for the PEG-MoS_2-AMP nanoplatform is weak at NIR light, the photothermal killing efficiency is low. After that, to find the photodynamic killing activity using the PEG-MoS_2-AMP nanoplatform with NIR light, we measured the ROS formation capability, using a reported method by us.[6,16,21,36] Figure 4B shows ROS formation from the PEG-MoS_2-AMP nanoplatform, during 670 nm NIR light exposure with comparison to buffer as a standard. Our experimental data indicate that the ROS formation amount is almost the same as in the presence and absence of the melittin antimicrobial peptide.

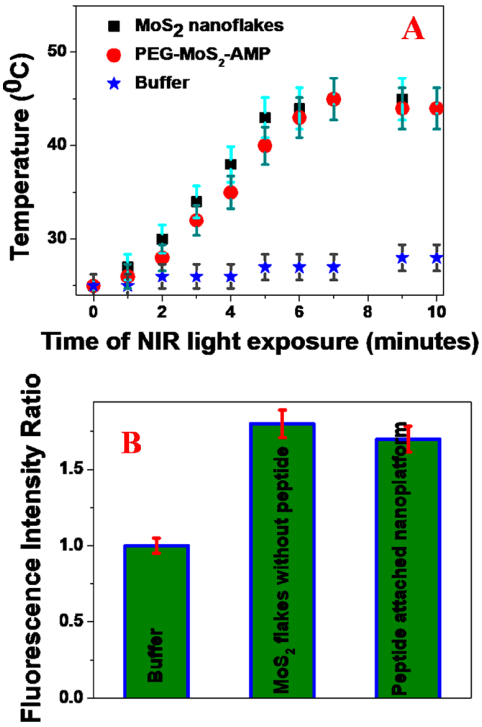

Figure 4. (A) Temperature change during photothermal killing of CRE *Escherichia coli* upon exposure to 670 nm light at the power of 1.3 W cm^{-2}. Temperature measurement performed in the presence of buffer, antimicrobial peptide-attached PEG-MoS_2-AMP nanoplatform, and PEG-MoS_2 nanoflakes only. (B) Plot showing ROS formation during killing of *E. coli* with NIR light in the presence of buffer and that PEG-MoS_2-AMP nanoplatform with or without the antimicrobial peptide.

To compare ROS formation activity with standard PDT dye, we performed the same experiment with ICG and our experimental results indicate that the ROS formation capability for the PEG-MoS_2-AMP nanoplatform is about 30% with respect to ICG. Our reported experimental data show that although our PEG-MoS_2-AMP nanoplatform is capable of PTT and PDT, due to the lower heat increase and smaller amount of ROS formation, only around 45% of MDRB were killed during combined PDT and PTT in the absence of the melittin antimicrobial peptide.

All of the above-reported experimental results indicate that less than 10% of superbugs can be killed by the melittin antimicrobial peptide. Similarly, around 45% of superbugs can be killed by PEG-MoS_2 nanoflakes without the melittin antimicrobial peptide. On the other hand, 100% of superbugs can be killed by the melittin antimicrobial peptide-attached PEG-MoS_2-AMP nanoplatform. Experimental data shows that the synergistic killing mechanism is responsible for 100% of MDRB killing. We believe that, in the presence of the melittin antimicrobial peptide-attached PEG-MoS_2-AMP nanoplatform, initially melittin antimicrobial peptides induce pore formation on the surface of superbugs. As reported before,[45−48] the melittin antimicrobial peptide induced pores on the surface of bacteria, which allow transmembrane leakage of molecules, as well as diffusion of atomic ions.[45−48] Due to the formation of pores by the melittin antimicrobial peptide, the PDT and PTT killing efficiency increased tremendously via the diffusion of heat and ROS very easily inside MDRB. As

DOI: 10.1021/acsabm.8b00632
ACS Appl. Bio Mater. 2019, 2, 769−776

a result, we observed 100% antibacterial efficiency in the presence of antimicrobial peptide-attached PEG-LA-MoS_2 QDs, upon exposure by 670 nm NIR light via a possible synergistic killing mechanism.

3. CONCLUSION

In conclusion, here, we reported the design of a novel nanoplatform using melittin antimicrobial peptide-attached MoS_2. Our reported data show that 100% of superbugs are killed using an antimicrobial peptide-attached PEG-MoS_2-AMP nanoplatform via a synergistic killing mechanism. Reported experimental data indicates that only 45% of MDRB killing is possible via MoS_2 nanoflake-based PTT and PDT processes together, and it is mainly due to the lower heat generation during PTT and a small amount of ROS formation during PDT in the presence of 670 nm light. Our reported data also show that about 20% of superbugs can be killed by the melittin antimicrobial peptide alone, whereas 100% of superbugs can be killed using melittin antimicrobial peptide-attached MoS_2 QDs with NIR light. This is due to the fact that, in the presence of the melittin antimicrobial peptide-attached PEG-MoS_2-AMP nanoplatform, initially the melittin antimicrobial peptide makes pores on the surface of MDRB, and the pores help to diffuse heat and ROS easily during PDT and PTT. Due to the possible synergistic multimodal killing mechanism, 100% of MDRB were killed.

■ ASSOCIATED CONTENT

Supporting Information

The Supporting Information is available free of charge on the ACS Publications website at DOI: 10.1021/acsabm.8b00632.

Synthesis of MoS_2 QDs, synthesis of melittin antimicrobial peptide-attached PEG-MoS_2-AMP nanoplatforms, MDRB sample preparation, size of MoS_2-PEG and only MoS_2 versus time, biocompatibility experiments for MoS_2-PEG and only MoS_2, MDRB bioimaging, PTT/PDT and chemical killing of MDRBs and finding the percentage of live MDRB, determination of minimum inhibitory concentrations, and ROS generation measurement during PDT (PDF)

■ AUTHOR INFORMATION

Corresponding Author

*E-mail: paresh.c.ray@jsums.edu. Fax: +16019793674.

Notes

The authors declare no competing financial interest.

■ ACKNOWLEDGMENTS

P.C.R. thanks NSF-PREM (grant no. DMR-1826886, DOD grant no. W911NF-16-1-0505, NSF CREST grant no. 1547754, NSF RISE grant no. 1547836, and NSF- RII-EPSCoR grant no. 1632899) for their generous funding.

■ REFERENCES

(1) *CDC 2018: Drug-Resistant "Nightmare Bacteria" Pose Growing Threat.* https://nypost.com/2018/04/03/drug-resistant-nightmare-bacteria-pose-growing-threat-cdc, (accessed, August 12, 2018).

(2) *World Health Organization.* http://www.who.int/mediacentre/factsheets/fs194/en/ (accessed August 8, 2018).

(3) Kavanagh, K. T.; Abusalem, S.; Calderon, L. E. The Incidence of MRSA Infections in the United States: is a More Comprehensive Tracking System Needed? *Antimicrob. Resist. In.* **2017**, *6*, 34.

(4) Qi, R.; Zhang, P.; Liu, J.; Zhou, L.; Zhou, C.; Zhang, N.; Han, Y.; Wang, S.; Wang, Y. Peptide Amphiphiles with Distinct Supramolecular Nanostructures for Controlled Antibacterial Activities. *ACS Appl. Bio Mater.* **2018**, *1*, 21−26.

(5) Zhu, S.; Yang, Y.; Bai, H.; Cui, Q.; Sun, H.; Li, L.; Wang, S.; Wang, X. Conjugated Polymer with Aggregation-Directed Intramolecular Förster Resonance Energy Transfer Enabling Efficient Discrimination and Killing of Microbial Pathogens. *Chem. Mater.* **2018**, *30*, 3244−3253.

(6) Vangara, A.; Pramanik, A.; Gao, Y.; Gates, K.; Begum, S.; Ray, P. C. Fluorescence Resonance Energy Transfer Based Highly Efficient Theranostic Nanoplatform for Two-Photon Bioimaging and Two-Photon Excited Photodynamic Therapy of Multiple Drug Resistance Bacteria. *ACS Appl. Bio Mater.* **2018**, *1*, 298−309.

(7) Ji, W. H.; Koepsel, R. R.; Murata, H.; Zadan, S.; Campbell, A. S.; Russell, A. J. Bactericidal Specificity and Resistance Profile of Poly(Quaternary Ammonium) Polymers and Protein-Poly-(Quaternary Ammonium) Conjugates. *Biomacromolecules* **2017**, *18*, 2583−2593.

(8) Yang, Y. C.; He, P.; Wang, Y. X.; Bai, H. T.; Wang, S.; Xu, J. F.; Zhang, X. Supramolecular Radical Anions Triggered by Bacteria In Situ for Selective Photothermal Therapy. *Angew. Chem., Int. Ed.* **2017**, *56*, 16239−16242.

(9) Zhao, Y.; Dai, X.; Wei, X.; Yu, Y.; Chen, X.; Zhang, X.; Li, C. Near-Infrared Light-Activated Thermosensitive Liposomes as Efficient Agents for Photothermal and Antibiotic Synergistic Therapy of Bacteria Film. *ACS Appl. Mater. Interfaces* **2018**, *10*, 14426−14437.

(10) Wang, B.; Feng, G. X.; Seifrid, M.; Wang, M.; Liu, B.; Bazan, G. C. Antibacterial Narrow-Band-Gap Conjugated Oligoelectrolytes with High Photothermal Conversion Efficiency. *Angew. Chem., Int. Ed.* **2017**, *56*, 16063−16066.

(11) Liu, S.; Yuan, H.; Bai, H.; Zhang, P.; Lv, F.; Liu, L.; Dai, Z.; Bao, J.; Wang, S. Electrochemiluminescence for Electric-Driven Antibacterial Therapeutics. *J. Am. Chem. Soc.* **2018**, *140*, 2284−2291.

(12) Dai, T.; Wang, C.; Wang, Y.; Xu, W.; Hu, J.; Cheng, Y. A Nanocomposite Hydrogel with Potent and Broad-Spectrum Antibacterial Activity. *ACS Appl. Mater. Interfaces* **2018**, *10*, 15163−15173.

(13) Chen, W.; Wang, Y.; Qin, M.; Zhang, X.; Zhang, Z.; Sun, X.; Gu, Z. Bacteria-Driven Hypoxia Targeting for Combined Biotherapy and Photothermal Therapy. *ACS Nano* **2018**, *12*, 5995−6005.

(14) Bai, H.; Lu, H.; Fu, X.; Zhang, E.; Lv, F.; Liu, L.; Wang, S. Supramolecular Strategy Based on Conjugated Polymers for Discrimination of Virus and Pathogens. *Biomacromolecules* **2018**, *19*, 2117−2122.

(15) Sinha, S. S.; Jones, S.; Pramanik, A.; Ray, P. C. Nanoarchitecture Based SERS for Biomolecular Fingerprinting and Label-Free Disease Markers Diagnosis. *Acc. Chem. Res.* **2016**, *49*, 2725−2735.

(16) Ray, P. C.; Khan, S. A.; Singh, A. K.; Senapati, D.; Fan, Z. Nanomaterials for Targeted Detection and Photothermal Killing of Bacteria. *Chem. Soc. Rev.* **2012**, *41*, 3193 −3209 .

(17) Jones, S.; Sinha, S. S.; Pramanik, A.; Ray, P. C. Three-dimensional (3D) Plasmonic Hot Spots for Label-free Sensing and Effective Photothermal Killing of Multiple Drug Resistant Superbugs. *Nanoscale* **2016**, *8*, 18301−18308.

(18) Viraka Nellore, B. P.; Kanchanapally, R.; Pedraza, F.; Sinha, S. S.; Pramanik, A.; Hamme, A. T.; Arslan, Z.; Sardar, D.; Ray, P. C. Bio-Conjugated Cnt-Bridged 3D Porous Graphene Oxide Membrane for Highly Efficient Disinfection of Pathogenic Bacteria and Removal of Toxic Metals from Water. *ACS Appl. Mater. Interfaces* **2015**, *7*, 19210−19218.

(19) Huang, J. L.; Zhou, J. F.; Zhuang, J. Y.; Gao, H. Z.; Huang, D. H.; Wang, L. X.; Wu, W. L.; Li, Q. B.; Yang, D.-P.; Han, M.-Y. Strong Near-Infrared Absorbing and Biocompatible CuS Nanoparticles for Rapid and Efficient Photothermal Ablation of Gram-Positive and -Negative Bacteria. *ACS Appl. Mater. Interfaces* **2017**, *9*, 36606−36614.

DOI: 10.1021/acsabm.8b00632
ACS Appl. Bio Mater. 2019, 2, 769−776

(20) Wang, Y. X.; Li, S. L.; Zhang, P. B.; Bai, H. T.; Feng, L. H.; Lv, F. T.; Liu, L. B.; Wang, S. Photothermal-Responsive Conjugated Polymer Nanoparticles for Remote Control of Gene Expression in Living Cells. *Adv. Mater.* **2018**, *30*, 1705418.
(21) Gao, Y.; Pramanik, A.; Begum, S.; Sweet, C.; Jones, S.; Alamgir, A.; Ray, P. C. Multifunctional Biochar for Highly Efficient Capture, Identification, and Removal of Toxic Metals and Superbugs from Water Samples. *ACS Omega* **2017**, *2*, 7730−7738.
(22) Tan, C.; Cao, X.; Wu, X.-J.; He, Q.; Yang, J.; Zhang, X.; Chen, J.; Zhao, W.; Han, S.; Nam, G.-H.; Sindoro, M.; Zhang, H. Recent Advances in Ultrathin Two-Dimensional Nanomaterials. *Chem. Rev.* **2017**, *117*, 6225−6331.
(23) Han, J. H.; Kwak, M.; Kim, Y.; Cheon, J. Recent Advances in the Solution-Based Preparation of Two-Dimensional Layered Transition Metal Chalcogenide Nanostructures. *Chem. Rev.* **2018**, *118*, 6151−6188.
(24) Sun, Y. G.; Alimohammadi, F.; Zhang, D. T.; Guo, G. S. Enabling Colloidal Synthesis of Edge-Oriented MoS_2 with Expanded Interlayer Spacing for Enhanced HER Catalysis. *Nano Lett.* **2017**, *17*, 1963−1969.
(25) Wachter, S.; Polyushkin, D. K.; Bethge, O.; Mueller, T. A Microprocessor Based on a Two-Dimensional Semiconductor. *Nat. Commun.* **2017**, *8*, 14948.
(26) Martella, C.; Mennucci, C.; Lamperti, A.; Cappelluti, E.; Buatier de Mongeot, F.; Molle, A. Designer Shape Anisotropy on Transition-Metal-Dichalcogenide Nanosheets. *Adv. Mater.* **2018**, *30*, 1705615.
(27) Wilson, N. R.; Nguyen, P. V.; Seyler, K.; Rivera, P.; Marsden, A. J.; Laker, Z. P. L.; Constantinescu, G. C.; Kandyba, V.; Barinov, A.; Hine, N. D. M.; Xu, X.; Cobden, D. H. Determination of Band Offsets, Hybridization, and Exciton Binding in 2D Semiconductor Heterostructures. *Sci. Adv.* **2017**, *3*, No. e1601832.
(28) Kang, J.; Sangwan, V. K.; Wood, J. D.; Hersam, M. C. Solution-Based Processing of Monodisperse Two-Dimensional Nanomaterials. *Acc. Chem. Res.* **2017**, *50*, 943−951.
(29) Manzeli, S.; Ovchinnikov, D.; Pasquier, D.; Yazyev, O. V.; Kis, A. 2D Transition Metal Dichalcogenides. *Nat. Rev. Mater.* **2017**, *2*, 17033.
(30) Chen, L.; Feng, Y.; Zhou, X.; Zhang, Q.; Nie, W.; Wang, W.; Zhang, Y.; He, C. One-Pot Synthesis of MoS_2Nanoflakes with Desirable Degradability for Photothermal Cancer Therapy. *ACS Appl. Mater. Interfaces* **2017**, *9*, 17347−17358.
(31) Liu, C.; Kong, D.; Hsu, P.-C.; Yuan, H.; Lee, H.-W.; Liu, Y.; Wang, H.; Wang, S.; Yan, K.; Lin, D.; Maraccini, P. A.; Parker, K. M.; Boehm, A. B.; Cui, Y. Rapid Water Disinfection Using Vertically Aligned MoS_2Nanofilms and Visible Light. *Nat. Nanotechnol.* **2016**, *11*, 1098−1104.
(32) Shen, S.; Chao, Y.; Dong, Z.; Wang, G.; Yi, X.; Song, G.; Yang, K.; Liu, Z.; Cheng, L. Bottom-Up Preparation of Uniform Ultrathin Rhenium Disulfide Nanosheets for Image-Guided Photothermal Radiotherapy. *Adv. Funct. Mater.* **2017**, *27*, 1700250.
(33) Kim, H.; Beack, S.; Han, S.; Shin, M.; Lee, T.; Park, Y.; Kim, K. S.; Yetisen, A. K.; Yun, S. H.; Kwon, W.; Hahn, S. K. Multifunctional Photonic Nanomaterials for Diagnostic, Therapeutic, and Theranostic Applications. *Adv. Mater.* **2018**, *30*, 1701460.
(34) Hao, J.; Song, G.; Liu, T.; Yi, X.; Yang, K.; Cheng, L.; Liu, Z. *In Vivo* Long-Term Biodistribution, Excretion, and Toxicology of PEGylated Transition-Metal Dichalcogenides MS_2 (M = Mo, W, Ti). Nanosheets. *Adv. Sci.* **2017**, *4*, 1600160.
(35) Dong, H.; Tang, S.; Hao, Y.; Yu, H.; Dai, W.; Zhao, G.; Cao, Y.; Lu, H.; Zhang, X.; Ju, H. Fluorescent MoS2Quantum Dots: Ultrasonic Preparation, Up-Conversion and Down-Conversion Bioimaging, and Photodynamic Therapy. *ACS Appl. Mater. Interfaces* **2016**, *8*, 3107−3114.
(36) Sweet, C.; Pramanik, A.; Jones, S.; Ray, P. C. Two-Photon Fluorescent Molybdenum Disulfide Dots for Targeted Prostate Cancer Imaging in the Biological II Window. *ACS Omega* **2017**, *2*, 1826−1835.
(37) Pandit, S.; Karunakaran, S.; Boda, S. K.; Basu, B.; De, M. High Antibacterial Activity of Functionalized Chemically Exfoliated MoS_2. *ACS Appl. Mater. Interfaces* **2016**, *8*, 31567−31573.
(38) Feng, Z.; Liu, X.; Tan, L.; Cui, Z.; Yang, X.; Li, Z.; Zheng, Y.; Yeung, K. W. K.; Wu, S. Electrophoretic Deposited Stable Chitosan@ MoS 2 Coating with Rapid In Situ Bacteria-Killing Ability under Dual-Light Irradiation. *Small* **2018**, *14*, 1704347.
(39) Amani, M.; Lien, D. H.; Kiriya, D.; Xiao, J.; Azcatl, A.; Noh, J.; Madhvapathy, S. R.; Addou, R.; Kc, S.; Dubey, M.; Cho, K.; Wallace, R. M.; Lee, S. C.; He, J. H.; Ager, J. W.; Zhang, X.; Yablonovitch, E.; Javey, M. Near-unity Photoluminescence Quantum Yield in MoS2. *Science* **2015**, *350*, 1065−1068.
(40) Li, L.; Yang, F.; Ye, G. J.; Zhang, Z.; Zhu, Z.; Lou, W.; Zhou, X.; Li, L.; Watanabe, K.; Taniguchi, T.; Chang, K.; Wang, Y.; Chen, X. H.; Zhang, Y. Quantum Hall Effect in Black Phosphorus Two-Dimensional Electron System. *Nat. Nanotechnol.* **2016**, *11*, 593−597.
(41) Peng, M. Y.; Zheng, D. W.; Wang, S. B.; Cheng, S. X.; Zhang, X. Multifunctional Nanosystem for Synergistic Tumor Therapy Delivered by Two-Dimensional MoS_2. *ACS Appl. Mater. Interfaces* **2017**, *9*, 13965−13975.
(42) Barua, S.; Dutta, H.; Gogoi, S.; Devi, R.; Khan, R. Nanostructured MoS_2-Based Advanced Biosensors: A Review. *ACS Appl. Nano Mater.* **2018**, *1*, 2−25.
(43) Zhang, X.; Lai, Z.; Tan, C.; Zhang, H. Solution-Processed Two Dimensional MoS2 Nanosheets: Preparation, Hybridization, and Applications. *Angew. Chem., Int. Ed.* **2016**, *55*, 8816−8838.
(44) Yin, W.; Yu, J.; Lv, F. T.; Yan, L.; Zheng, L. R.; Gu, Z. J.; Zhao, Y. L. Functionalized Nano-MoS_2 with Peroxidase Catalytic and Near-Infrared Photothermal Activities for Safe and Synergetic Wound Antibacterial Applications. *ACS Nano* **2016**, *10*, 11000−11011.
(45) Kanchanapally, R.; Nellore, B. P. V.; Sinha, S. S.; Pedraza, F.; Jones, S. J.; Pramanik, A.; Chavva, S. R.; Tchounwou, C.; Shi, Y.; Vangara, A.; Sardar, D.; Ray, P. C. Antimicrobial Peptide-Conjugated Graphene Oxide Membrane for Efficient Removal and Effective Killing of Multiple Drug Resistant Bacteria. *RSC Adv.* **2015**, *5*, 18881−18887.
(46) Adade, C. M.; Oliveira, I. R. S.; Pais, J. A. R.; Souto-Padron, T. Melittin Peptide Kills Trypanosoma Cruzi Parasites by Inducing Different Cell Death Pathways. *Toxicon* **2013**, *69*, 227−−239.
(47) Gajski, G.; Garaj-Vrhovac, V. Melittin: A Lytic Peptide with Anticancer Properties. *Environ. Toxicol. Pharmacol.* **2013**, *36*, 697−705.
(48) Boyce, J. M.; Pop, O.-F.; Abreu-Lanfranco, O.; Hung, W. Y.; Fisher, A.; Karjoo, A.; Thompson, B.; Protopapas, Z. A Trial of Discontinuation of Empiric Vancomycin Therapy in Patients with Suspected Methicillin-Resistant Staphylococcus aureus Health Care-associated Pneumonia. *Antimicrob. Agents Chemother.* **2013**, *57*, 1163−1168.

DOI: 10.1021/acsabm.8b00632
ACS Appl. Bio Mater. 2019, 2, 769−776